Liquid Metal-Tunable Miniaturized Bimodal Cavity for Enhanced Measurement Accuracy in the ISM Bands

Anıl Karatay; Fatih Yaman

Published version information

Citation: A. Karatay and F. Yaman, "Liquid Metal-Tunable Miniaturized Bimodal Cavity for Enhanced Measurement Accuracy in the ISM Bands," in IEEE Transactions on Instrumentation and Measurement, vol. 73, pp. 1-9, 2024, Art no. 8001009

DOI: https://doi.org/10.1109/TIM.2023.3343801

Liquid metal-tunable miniaturized bimodal cavity for enhanced measurement accuracy in the ISM bands

Anıl Karatay and Fatih Yaman *

Abstract

Enhancing measurement accuracy or reducing the effect of the neighboring modes in resonant cavities may necessitate the separation of mode frequencies. However, in ISM-band measurement configurations utilizing a rectangular or cylindrical cavity, the placement of the first two modes at 2.45 and 5.8 GHz is unattainable, necessitating the presence of additional modes in between that would potentially degrade measurement accuracy. This article begins with an analytical approach, employing Lagrange multipliers for the first time to reveal the level of separation achievable in the frequency domain between the initial two modes within these types of conventional cavities. The analytical results were also verified with a numerical grid search. Subsequently, innovative strategies have been introduced to surpass this intrinsic constraint that reduces the measurement accuracy in various applications. A novel minizaturized cavity configuration has been proposed to operate bimodally at 2.45 and 5.8 GHz and manufactured with a 3D printer. It has been ensured that there are no physical modes present in between, and measurements of the structure have been conducted. Another notable innovation of the article is the capability of tuning the proposed cavity structure by means of liquid metal displacement. Thus, a more flexible tuning method compared to mechanical tuning techniques can be achieved, enabling precise adjustment of the desired measurement frequency. Good agreement between the simulation and measurement results has been reported.

Microwave cavities, Analytical and numerical methods, Additive manufacturing, Liquid metal, Enhanced accuracy

1 Introduction

Microwave cavities play a crucial role in a wide range of contemporary measurement technologies, including dielectric permittivity measurements [1–5], permeability

*The authors are with the Department of Electrical and Electronics Engineering, İzmir Institute of Technology, Urla, İzmir, 35430 Türkiye. F. Yaman is also with ASTeC, STFC, Daresbury Laboratory, Warrington, UK. e-mail: anilkaratay@iyte.edu.tr.

measurements [6,7], thickness determination [8] and electron density measurement [9]. In addition to the aforementioned applications, microwave cavities also play a vital role in other cutting-edge technologies [10–13]. As resonant structures, they are engineered to confine electromagnetic waves within a specific volume, leading to the creation of resonant modes with distinct resonant frequencies. Microwave cavity modes signify the specific resonant frequencies at which electromagnetic waves can resonate within a confined metallic structure. These modes possess unique positions in the frequency domain, separated by a designated frequency interval, which is determined by the dimensions and form of the cavity [14].

In many studies in the literature, the excitation of only one mode while removing other modes has been desired. In single-band dielectric permittivity measurements [4], non-resonant permittivity measurements performed inside the cavity [5], single mode type heating cavities [15, 16], some accelerator applications [17], it has been aimed to separate the mode frequencies from each other to a sufficient extent. Particularly in measurements inducing frequency shifts or reducing quality factors, the overlapping of spectral peaks related to modes is a frequently encountered problem. That is why the separation of the first and second modes in a cavity has several benefits, including improved signal isolation, suppressed nonlinearities, increased control over mode frequencies during the measurement process, and enhanced measurement accuracy. The measurement system's accuracy and precision are improved as intermodal crosstalk is diminished.

In this context, separating the mode frequencies from each other to a sufficient degree has become a critical problem for enhanced measurement accuracy. Firstly, it has been analytically demonstrated that a constraint exists in separating the initial two modes within conventional cavities, and the limit is insufficient for the placement of the first two modes at 2.45 and 5.8 GHz within the ISM bands. The maximum ratio of the first two modes in conventional cavities can be determined using various charts and numerical methods [18]; however, the analytical representation utilizing Lagrange multipliers, to the best of our knowledge, was first established in this study. In a conventional rectangular or cylindrical cavity, while the first mode settles at 2.45 GHz, it has been analytically demonstrated and verified that the second mode cannot be positioned at 5.8 GHz. For this reason, we have proposed a novel miniaturized cavity enabling the placement of the first mode at 2.45 GHz and the second mode at 5.8 GHz while simultaneously eliminating all potential modes within the intervening frequencies on the physical and mathematical bases. The cavity, entirely constructed using additive manufacturing techniques similar to specific cavity instruments in the literature [19, 20], underwent foundational electromagnetic tests. Additionally, a liquid metal-assisted approach has been employed to compensate for minor frequency shifts observed in resonant frequencies stemming from production errors or various other issues. Liquid metal materials, previously utilized for specific antenna configurations in the literature [21], have been employed in this study as tuners for a 3D cavity structure resulting in a more versatile system.

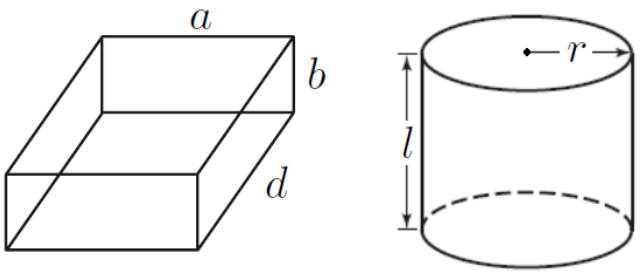

Figure 1: The structures of the rectangular and cylindrical cavities

2 Analytical Calculations

This section is devoted to analytically determining the upper limit of the ratio between the first two modes of rectangular and cylindrical cavities. The structures of the cavities are depicted in Fig. 1.

2.1 Rectangular Cavity

The resonant frequency of any Transverse Electric (TE) or Transverse Magnetic (TM) mode of a rectangular cavity can be calculated as shown in Equation 1.

$$f_{mnp} = \frac{c}{2\pi\sqrt{\epsilon_r \mu_r}} \sqrt{\left(\frac{m\pi}{a}\right)^2 + \left(\frac{n\pi}{b}\right)^2 + \left(\frac{p\pi}{d}\right)^2} \tag{1}$$

where c denotes the speed of light, ϵ_r and μ_r are the relative permittivity and permeability, respectively. a, b, and d are the cavity dimensions under the assumption that $b \leq a \leq d$. m, n, and p are the integers that represent the cavity modes [18].

The dominant mode of a rectangular cavity is the TE_{101} mode when using the previous assumption related to the dimensions and considering that at most one of the values m, n, and p can be zero. The potential second modes in a rectangular cavity are identified as the TE_{011} or TE_{102} modes. The main objective here is to determine the value at which the ratio of the second mode to the first mode is maximized.

$$max\left\{\frac{min\{f_{011},\ f_{102}\}}{f_{101}}\right\},\ b \leq\ a \leq d \tag{2}$$

First, we need to determine whether the second mode is TE_{011} or TE_{102}. The mode with the smaller frequency of f_{011} and f_{102} will be the second mode, so we need to consider the cases where one of these two values is smaller than the other.

$$f_{011} \lessgtr f_{102} \tag{3}$$

By taking the square of both sides, we can get rid of the square root.

$$\left(\frac{1}{b}\right)^2 + \left(\frac{1}{d}\right)^2 \lessgtr \left(\frac{1}{a}\right)^2 + \left(\frac{2}{d}\right)^2 \tag{4}$$

$$\frac{1}{b^2} - \frac{1}{a^2} - \frac{3}{d^2} \lesseqgtr 0 \tag{5}$$

Under such circumstances, if $\frac{1}{b^2} - \frac{1}{a^2} - \frac{3}{d^2}$ is greater than or equal to zero, the second mode is TE_{102}, otherwise it is TE_{011}.

Case I: If $\frac{1}{b^2} - \frac{1}{a^2} - \frac{3}{d^2} \geq 0$, TE_{102} is the second mode. We will minimize $\left(\frac{f_{101}}{f_{102}}\right)^2$ with the constraints of $\frac{1}{b^2} - \frac{1}{a^2} - \frac{3}{d^2} \geq 0$, $b - a \leq 0$, $a - d \leq 0$, $b > 0$, $a > 0$, $d > 0$. Minimizing the square of the multiplicative inverse of the function will also lead us to the same result we aim to maximize. Three slack variables, namely q^2, s^2, and t^2, shall be introduced, subject to the constraint that they are non-negative, to represent the limitations imposed by three inequality constraints. If we define the dimension vector as $\vec{r} = [a\ b\ d]^T$, the function to be minimized and its constraints can be written as follows.

$$Minimize\ g(\vec{r}) = \frac{\left(\frac{1}{a}\right)^2 + \left(\frac{1}{d}\right)^2}{\left(\frac{1}{a}\right)^2 + \left(\frac{2}{d}\right)^2} \tag{6}$$

$$Subject\ to\ h_1(\vec{r}, q) = \frac{1}{b^2} - \frac{1}{a^2} - \frac{3}{d^2} - q^2 = 0 \tag{7}$$

$$h_2(\vec{r}, s) = b - a + s^2 = 0 \tag{8}$$

$$h_3(\vec{r}, t) = a - d + t^2 = 0 \tag{9}$$

where $a, b, d > 0$. The Lagrangian function can be written as:

$$L(\vec{r}, \vec{\lambda}) = g(\vec{r}) - \lambda_1 h_1(\vec{r}, q) - \lambda_2 h_2(\vec{r}, s) - \lambda_3 h_3(\vec{r}, t) \tag{10}$$

where $\vec{\lambda} = [\lambda_1\ \lambda_2\ \lambda_3]^T$ denotes the Lagrange multiplier vector. $\nabla_{\vec{r},\vec{\lambda}} L = 0$ while the constraints are satisfied.

$$\frac{\partial L}{\partial a} = \frac{-6ad^2}{\left(4a^2 + d^2\right)^2} - \frac{2\lambda_1}{a^3} + \lambda_2 - \lambda_3 = 0 \tag{11}$$

$$\frac{\partial L}{\partial b} = \frac{2\lambda_1}{b^3} - \lambda_2 = 0 \tag{12}$$

$$\frac{\partial L}{\partial d} = \frac{6a^2 d}{\left(4a^2 + d^2\right)^2} - \frac{6\lambda_1}{d^3} + \lambda_3 = 0 \tag{13}$$

$$\frac{\partial L}{\partial \lambda_1} = -\frac{1}{b^2} + \frac{1}{a^2} + \frac{3}{d^2} + q^2 = 0 \tag{14}$$

$$\frac{\partial L}{\partial \lambda_2} = -b + a - s^2 = 0 \tag{15}$$

$$\frac{\partial L}{\partial \lambda_3} = -a + d - t^2 = 0 \tag{16}$$

By satisfying the complementary slackness condition, we can reach the optimal solution for this problem [22].

i) $q = 0,\ s = 0,\ t = 0,\ \lambda_1 \neq 0,\ \lambda_2 \neq 0,\ \lambda_3 \neq 0$
In this scenario, Equations 15 and 16 yield $a = b = d$. However, Equation 14 is not satisfied as q equals to zero and d must be greater than zero.

ii) $q \neq 0,\ s \neq 0,\ t \neq 0,\ \lambda_1 = 0,\ \lambda_2 = 0,\ \lambda_3 = 0$
Given that $a, b, d > 0$, Equations 11 and 13 are not fulfilled.

iii) $q \neq 0,\ s = 0,\ t = 0,\ \lambda_1 = 0,\ \lambda_2 \neq 0,\ \lambda_3 \neq 0$
Equation 12 is not met in this case.

iv) $q = 0,\ s \neq 0,\ t = 0,\ \lambda_1 \neq 0,\ \lambda_2 = 0,\ \lambda_3 \neq 0$
Equation 12 remains unfulfilled.

v) $q = 0,\ s = 0,\ t \neq 0,\ \lambda_1 \neq 0,\ \lambda_2 \neq 0,\ \lambda_3 = 0$
In this scenario, Equation 15 results in $a = b$. However, Equation 14 is not satisfied as $q = 0$ and $d > 0$.

vi) $q = 0,\ s \neq 0,\ t \neq 0,\ \lambda_1 \neq 0,\ \lambda_2 = 0,\ \lambda_3 = 0$
Equation 12 is not satisfied.

vii) $q \neq 0,\ s = 0,\ t \neq 0,\ \lambda_1 = 0,\ \lambda_2 \neq 0,\ \lambda_3 = 0$
Equation 12 remains unfulfilled.

viii) $q \neq 0,\ s \neq 0,\ t = 0,\ \lambda_1 = 0,\ \lambda_2 = 0,\ \lambda_3 \neq 0$
In this scenario, Equation 16 results in $a = d$, and Equation 14 can be utilized to obtain $b < (a/2)$. All other equations, including Equation 11 and 13 with the same λ_3 value, can also be satisfied under these conditions. As such, $a = d > 2b$ represents the optimal solution for this case.

When we select any value that satisfies the condition $a = d > 2b$ for the function f_{102}/f_{101}, the resulting value is $\sqrt{5/2}$.
Case II: If $\frac{1}{b^2} - \frac{1}{a^2} - \frac{3}{d^2} \leq 0$, TE_{011} is the second mode. In Case II, we are going to minimize $\left(\frac{f_{101}}{f_{011}}\right)^2$ with the constraints of $\frac{1}{b^2} - \frac{1}{a^2} - \frac{3}{d^2} \leq 0$, $b - a \leq 0$, $a - d \leq 0$, $b > 0$, $a > 0$, $d > 0$.

$$Minimize\ g(\vec{r}) = \frac{\left(\frac{1}{a}\right)^2 + \left(\frac{1}{d}\right)^2}{\left(\frac{1}{b}\right)^2 + \left(\frac{1}{d}\right)^2} \tag{17}$$

$$Subject\ to\ h_1(\vec{r}, q) = \frac{1}{b^2} - \frac{1}{a^2} - \frac{3}{d^2} + q^2 = 0 \tag{18}$$

$$h_2(\vec{r}, s) = b - a + s^2 = 0 \tag{19}$$

$$h_3(\vec{r}, t) = a - d + t^2 = 0 \tag{20}$$

$$\frac{\partial L}{\partial a} = \frac{-2}{a^3\left(\left(\frac{1}{b}\right)^2 + \left(\frac{1}{d}\right)^2\right)} - \frac{2\lambda_1}{a^3} + \lambda_2 - \lambda_3 = 0 \tag{21}$$

$$\frac{\partial L}{\partial b} = \frac{2bd^2\left(a^2 + d^2\right)}{a^2\left(b^2 + d^2\right)^2} + \frac{2\lambda_1}{b^3} - \lambda_2 = 0 \tag{22}$$

$$\frac{\partial L}{\partial d} = \frac{2b^2 d\left(b^2 - a^2\right)}{a^2\left(b^2 + d^2\right)^2} - \frac{6\lambda_1}{d^3} + \lambda_3 = 0 \tag{23}$$

$$\frac{\partial L}{\partial \lambda_1} = -\frac{1}{b^2} + \frac{1}{a^2} + \frac{3}{d^2} - q^2 = 0 \tag{24}$$

$$\frac{\partial L}{\partial \lambda_2} = -b + a - s^2 = 0 \tag{25}$$

$$\frac{\partial L}{\partial \lambda_3} = -a + d - t^2 = 0 \tag{26}$$

For the sake of simplicity, only the satisfied conditions will be written in the upcoming cases and the following results will emerge:

i) $q = 0,\ s \neq 0,\ t = 0,\ \lambda_1 \neq 0,\ \lambda_2 = 0,\ \lambda_3 \neq 0$
From Equations 24 and 26, $a = d = 2b$. By isolating the value of λ_1 in Equation 22 and expressing the values of a and d in terms of b, λ_1 can be determined to be $-(8b^2)/25$. Under these conditions, λ_3 simultaneously satisfies Equations 21 and 23. Therefore, this scenario is a candidate for a feasible solution.

ii) $q \neq 0,\ s = 0,\ t \neq 0,\ \lambda_1 = 0,\ \lambda_2 \neq 0,\ \lambda_3 = 0$
As per Equations 25 and 26, it is stated that $a = b < d$. As a result of $a = b$, Equation 23 is satisfied. Given that $\lambda_1 = \lambda_3 = 0$, λ_2 must satisfy both Equation 21 and Equation 22. The solution to this scenario is when λ_2 takes the value of $(2d^2)/(a^3 + ad^2)$, fulfilling both equations. This scenario therefore represents another candidate as a feasible solution.

When we place the values we found into the function $g(\vec{r}) = (f_{101}/f_{011})^2$, scenario i gives a value of 0.4 (min) while scenario ii gives a value of 1 (max). If we substitute the value in scenario i to the function f_{011}/f_{101}, we will reach the value of $\sqrt{5/2} \approx 1.581$ in which we found the same value in Case I. This is the upper limit for the separability of the first two modes in a rectangular cavity.

2.2 Cylindrical Cavity

The resonant frequency of a hollow cylindrical cavity can be calculated as follows.

$$f_{nmp} = \frac{c}{2\pi}\sqrt{\left(\frac{\chi_{nm}}{r}\right)^2 + \left(\frac{p\pi}{l}\right)^2} \tag{27}$$

where r and l denote the radius and height of the cylindrical cavity, respectively. χ denotes the roots of Bessel functions for TM modes and the roots of the derivative of Bessel functions for TE modes.

The dominant mode of a cylindrical cavity can either be TE_{111} or TM_{010}, depending on the ratio of the diameter to the height of the cavity. If the dominant mode is TE_{111}, the possible second modes are TE_{112} or TM_{010}. In the other case, the possible second modes are TE_{111} or TM_{110}. $\chi_{11}^{(TE)}$, $\chi_{01}^{(TM)}$, and $\chi_{11}^{(TM)}$ are 1.841, 2.405 and 3.832, respectively. We need to determine whether

the dominant mode is TE_{111} or TM_{010}. The mode with the smaller frequency of f_{TE111} and f_{TM010} will be the dominant mode, so we need to consider the cases where one of these values is smaller.

$$f_{TE111} \lessgtr f_{TM010} \tag{28}$$

$$\left(\frac{1.841}{r}\right)^2 + \left(\frac{\pi}{l}\right)^2 \lessgtr \left(\frac{2.405}{r}\right)^2 \tag{29}$$

$$\frac{-2.395}{r^2} + \frac{\pi^2}{l^2} \lessgtr 0 \tag{30}$$

The dominant mode is TE_{111} if the expression in Equation 30 is less than zero, otherwise it is TM_{010}. In this cavity, there are two cases for the dominant modes and two second mode cases for each dominant mode, so a total of four different cases will be analyzed under different constraints. Cases for different scenarios of the dominant mode are named with capital letters. For the different scenarios of the second mode, Roman numerals are used, as in the rectangular cavity.

Case A: If $\frac{-2.395}{r^2} + \frac{\pi^2}{l^2} \geq 0$, the dominant mode is TM_{010}. The problem to be solved for this case can be written as follows.

$$max\left\{\frac{min\{f_{TE111},\ f_{TM110}\}}{f_{TM010}}\right\} \tag{31}$$

First, we need to determine whether the second mode is TE_{111} or TM_{110} in this case. The mode with the smaller frequency will be the second mode.

$$f_{TM110} \lessgtr f_{TE111} \tag{32}$$

$$\left(\frac{3.832}{r}\right)^2 \lessgtr \left(\frac{1.841}{r}\right)^2 + \left(\frac{\pi}{l}\right)^2 \tag{33}$$

$$\frac{11.295}{r^2} - \frac{\pi^2}{l^2} \lessgtr 0 \tag{34}$$

The second mode in Case A is TE_{111} if the expression in Equation 34 is greater than or equal zero, otherwise it is TM_{110}.

Case A-I: Considering that $\frac{-2.395}{r^2} + \frac{\pi^2}{l^2} \geq 0$ and $\frac{11.295}{r^2} - \frac{\pi^2}{l^2} \geq 0$, the dominant mode is TM_{010} and the second mode is TE_{111}. We will minimize $(f_{TM010}/f_{TE111})^2$ with two slack variables.

$$Minimize\ g(\vec{\phi}) = \frac{\left(\frac{2.405}{r}\right)^2}{\left(\frac{1.841}{r}\right)^2 + \left(\frac{\pi}{l}\right)^2} = \frac{\frac{5.784}{r^2}}{\frac{3.389}{r^2} + \frac{\pi^2}{l^2}} \tag{35}$$

$$Subject\ to\ h_1(\vec{\phi}, q) = \frac{-2.395}{r^2} + \frac{\pi^2}{l^2} - q^2 = 0 \tag{36}$$

$$h_2(\vec{\phi}, s) = \frac{11.295}{r^2} - \frac{\pi^2}{l^2} - s^2 = 0 \tag{37}$$

where $\vec{\phi} = [r\ l]^T$ and $r,\ l > 0$.

$$L(\vec{\phi}, \vec{\lambda}) = g(\vec{\phi}) - \lambda_1 h_1(\vec{\phi}, q) - \lambda_2 h_2(\vec{\phi}, s) \tag{38}$$

$$\frac{\partial L}{\partial r} = \frac{-9.94065 l^2 r}{\left(l^2 + 2.91225 r^2\right)^2} - \frac{4.79\lambda_1}{r^3} + \frac{22.59\lambda_2}{r^3} = 0 \tag{39}$$

$$\frac{\partial L}{\partial l} = \frac{9.94065 l r^2}{\left(l^2 + 2.91225 r^2\right)^2} + \frac{2\pi^2\left(\lambda_1 - \lambda_2\right)}{l^3} = 0 \tag{40}$$

$$\frac{\partial L}{\partial \lambda_1} = \frac{2.395}{r^2} - \frac{\pi^2}{l^2} + q^2 = 0 \tag{41}$$

$$\frac{\partial L}{\partial \lambda_2} = \frac{-11.295}{r^2} + \frac{\pi^2}{l^2} + s^2 = 0 \tag{42}$$

The satisfied conditions are given below.

i) $q \neq 0,\ s = 0,\ \lambda_1 = 0,\ \lambda_2 \neq 0$
As per Equation 42, the value of r is approximately equal to $1.07l$. Upon incorporating this result into Equations 39 and 40, all equations are fulfilled.

ii) $q = 0,\ s \neq 0,\ \lambda_1 \neq 0,\ \lambda_2 = 0$
As determined by Equation 41, the value of r is approximately $0.4926l$. Upon substitution of this value into Equations 39 and 40, all equations are satisfied.

The function that we aim to minimize is $(f_{TM010}/f_{TE111})^2$, thus the related point would give the maximum of f_{TE111}/f_{TM010}. By placing the values from conditions i and ii into the f_{TE111}/f_{TM010} function, it was found that the ratio of these two values can be a minimum of 1 according to condition ii, and a maximum of ~ 1.593 according to condition i.
Case A-II: Assuming $\frac{-2.395}{r^2} + \frac{\pi^2}{l^2} \geq 0$ and $\frac{11.295}{r^2} - \frac{\pi^2}{l^2} \leq 0$, the dominant mode is TM_{010} and the second mode is TM_{110}.

$$Maximize\ \frac{f_{TM110}}{f_{TM010}} = \frac{\frac{3.832c}{2\pi r}}{\frac{2.405c}{2\pi r}} = \frac{3.832}{2.405} \approx 1.593 \tag{43}$$

In this case, the obtained ratio remains constant regardless of the values of r and l, thus no further manipulation is required. Consistent with the maximum value obtained in the previous case, the maximum value was again found to be approximately 1.593.
Case B: If $\frac{-2.395}{r^2} + \frac{\pi^2}{l^2} \leq 0$, the dominant mode is TE_{111}. The problem to be solved for this case:

$$max\left\{\frac{min\{f_{TE112},\ f_{TM010}\}}{f_{TE111}}\right\} \tag{44}$$

We must determine whether the second mode is TE_{112} or TM_{010} while the dominant mode is TE_{111}.

$$f_{TM010} \lessgtr f_{TE112} \tag{45}$$

$$\left(\frac{2.405}{r}\right)^2 \lessgtr \left(\frac{1.841}{r}\right)^2 + \left(\frac{2\pi}{l}\right)^2 \tag{46}$$

$$\frac{2.395}{r^2} - \frac{4\pi^2}{l^2} \lessgtr 0 \tag{47}$$

In the case that the expression attains a non-negative value, the second mode is TE_{112}. Conversely, if the expression is less than zero, the second mode is TM_{010}.

Case B-I: Given the constraints $\frac{-2.395}{r^2} + \frac{\pi^2}{l^2} \leq 0$ and $\frac{2.395}{r^2} - \frac{4\pi^2}{l^2} \leq 0$, the dominant mode of oscillation is determined to be TE_{111} and the second mode is TM_{010}. For the sake of computational ease, we will instead opt to maximize the square of the relevant ratio directly, without requiring a multiplicative inversion. As a result, we will endeavor to maximize the function $(f_{TM010}/f_{TE111})^2$ within the confines of these constraints.

$$Maximize\ g(\vec{\phi}) = \frac{\left(\frac{2.405}{r}\right)^2}{\left(\frac{1.841}{r}\right)^2 + \left(\frac{\pi}{l}\right)^2} = \frac{\frac{5.784}{r^2}}{\frac{3.389}{r^2} + \frac{\pi^2}{l^2}} \tag{48}$$

$$Subject\ to\ h_1(\vec{\phi}, q) = \frac{-2.395}{r^2} + \frac{\pi^2}{l^2} + q^2 = 0 \tag{49}$$

$$h_2(\vec{\phi}, s) = \frac{2.395}{r^2} - \frac{4\pi^2}{l^2} + s^2 = 0 \tag{50}$$

$$\frac{\partial L}{\partial r} = \frac{-9.94065 l^2 r}{\left(l^2 + 2.91225 r^2\right)^2} - \frac{4.79\lambda_1}{r^3} + \frac{4.79\lambda_2}{r^3} = 0 \tag{51}$$

$$\frac{\partial L}{\partial l} = \frac{9.94065 l r^2}{\left(l^2 + 2.91225 r^2\right)^2} + \frac{2\pi^2\left(\lambda_1 - 4\lambda_2\right)}{l^3} = 0 \tag{52}$$

$$\frac{\partial L}{\partial \lambda_1} = \frac{2.395}{r^2} - \frac{\pi^2}{l^2} - q^2 = 0 \tag{53}$$

$$\frac{-2.395}{r^2} + \frac{4\pi^2}{l^2} - s^2 = 0 \tag{54}$$

i) $q \neq 0,\ s = 0,\ \lambda_1 = 0,\ \lambda_2 \neq 0$
Using Equation 54, we obtain $r = 0.2463l$. Upon substituting this value into Equations 51 and 52, all the equations are fulfilled.

ii) $q = 0,\ s \neq 0,\ \lambda_1 \neq 0,\ \lambda_2 = 0$
According to Equation 53, the value of r is calculated to be approximately $0.4926l$. Upon substituting this value into Equations 51 and 52, all the equations are satisfied.

By substituting the relationships in conditions i and ii into Equation 48, the maximum value of f_{TM010}/f_{TE111} under these constraints was approximately 1.20 under condition i. The value found under condition ii was 1. However, 1.20 is smaller than 1.593 found in Case A, and thus, it does not indicate the global extremum for the entire problem.

Case B-II: The constraints are defined as $\frac{-2.395}{r^2} + \frac{\pi^2}{l^2} \leq 0$ and $\frac{2.395}{r^2} - \frac{4\pi^2}{l^2} \geq 0$. The first constraint yields the inequality $r \leq 0.4926l$, and the second constraint results in $r \leq 0.2463l$. If the second constraint is satisfied, it is guaranteed that the first constraint is satisfied as well, so there is no need to include the first constraint in the process. It is noteworthy in Case B-II that the dominant mode is TE_{111} and the second mode is TE_{112}.

$$Maximize\ g(\vec{\phi}) = \left(\frac{f_{TE112}}{f_{TE111}}\right)^2 = \frac{\left(\frac{1.841}{r}\right)^2 + \left(\frac{2\pi}{l}\right)^2}{\left(\frac{1.841}{r}\right)^2 + \left(\frac{\pi}{l}\right)^2} \tag{55}$$

$$Subject\ to\ h_1(\vec{\phi}, q) = \frac{2.395}{r^2} - \frac{4\pi^2}{l^2} - q^2 = 0 \tag{56}$$

$$L(\vec{\phi}, \lambda_1) = g(\vec{\phi}) - \lambda_1 h_1(\vec{\phi}, q) \tag{57}$$

$$\frac{\partial L}{\partial r} = \frac{17.472l^2 r}{\left(l^2 + 2.91201r^2\right)^2} + \frac{4.79\lambda_1}{r^3} = 0 \tag{58}$$

$$\frac{\partial L}{\partial l} = \frac{-17.472lr^2}{\left(l^2 + 2.91201r^2\right)^2} - \frac{8\pi^2\lambda_1}{l^3} = 0 \tag{59}$$

$$\frac{\partial L}{\partial \lambda_1} = \frac{-2.395}{r^2} + \frac{4\pi^2}{l^2} + q^2 = 0 \tag{60}$$

i) $q = 0,\ \lambda_1 \neq 0$
We find that the value of $\frac{f_{TE112}}{f_{TE111}}$ is 1.20 similar to the previous case under the assumption that $r = 0.2463l$. Although this value represents a solution for this case, upon considering all the other cases, it is not the maximum ratio.

Analytically it has been proven that, the frequency of the second mode of a cylindrical cavity can be at most ~ 1.593 times that of the first mode.

3 Numerical Verification

This section is dedicated to the numerical verification of the analytical results obtained in the previous section. In order to fulfill the condition $b \leq a \leq d$ for the rectangular cavity and to facilitate visualization, the value of b is fixed at 0.05 m, and the values of a and d are calculated, starting from 0.05 m and without breaking the constraint $a \leq d$.

For this procedure, the resonant frequencies of the TE_{101}, TE_{102}, and TE_{011} modes were calculated within two nested loops that change the values of a and d

from 0.05 m to 1 m, and the obtained values were stored in a vector and sorted in ascending order at each iteration step. At each iteration step, the ratio of the second value to the first value of the relevant vector was calculated, and the values that this ratio took were plotted in Fig. 2-(a). As can be seen in this figure, the highest value obtained in the region where the constraint $a \leq d$ is fulfilled is 1.581. As demonstrated analytically, the maximum value is obtained when b is small enough, and a equals d. The parts where the constraint $a \leq d$ is not satisfied are shown as zero in the surface plot.

A similar procedure was also applied for the cylindrical cavity. Unlike the rectangular cavity, there is no superiority between the values of r and l, so a free-form search was carried out. Both values were scanned from 0.05 m to 1 m, and the possible dominant and secondary modes were calculated for each pair of values. At each step, the ratio of the second value to the first value among the frequency values sorted in ascending order is shown in Fig. 2-(b). Numerically, the ratio of the frequency of the second mode to that of the first mode has been found to be 1.593 in accordance with the analytical result. It is possible for small differences to occur in the fourth decimal place and beyond in the analytical calculation due to simple rounding performed in the square root and square operations. The local maximum of 1.2, which is obtained in Case B-I and Case B-II, is clearly visible in Fig. 2-(b). The grid search results also show that the global minimum of 1, which is the optimal value for both problems, can be observed.

4 Experimental Verification and Surpassing the Limit

This section is devoted to experimentally demonstrating the results and exceeding the limits found in previous sections. After that, a miniaturized splitted-mode cavity configuration is demonstrated.

4.1 Mechanical Perturbation with a Metallic Object

Changing the boundary condition to either the inward or outward direction along the surface normal of the cavity will result in a shift of the frequency either upward or downward. Furthermore, the directions of frequency shift is dependent on the region where the boundaries of the cavity are changed, see Equation 61 [23].

$$\frac{\omega_u - \omega_p}{\omega_u} \approx \frac{\Delta W_e - \Delta W_m}{W} \tag{61}$$

where ω_u and ω_p are angular resonant frequency of unperturbed cavity and that of the perturbed cavity, respectively. ΔW_e denotes the alteration in the stored electric energy, ΔW_m indicates the alteration in the stored magnetic energy, and W is the total stored energy.

The electric field value of the first mode and the magnetic field value of the second mode peak at the center. In contrast, the magnetic field value of

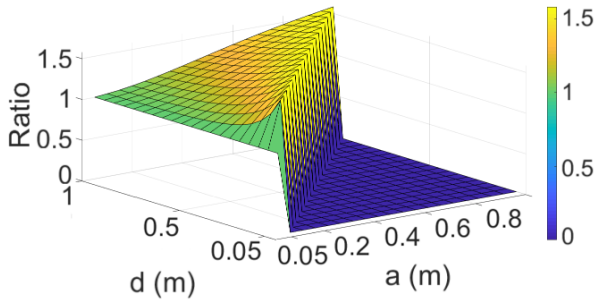

(a)

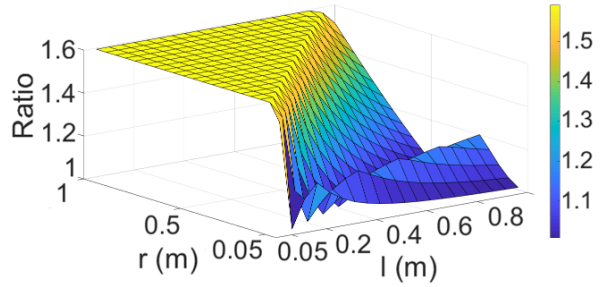

(b)

Figure 2: The ratio of the resonant frequency of the second mode to that of the first mode of (a) rectangular (b) cylindrical cavity

the first mode and the electric field value of the second mode approach zero near the center of the cavities. In this context, a perturbation applied inward from the center of the cavity will reduce the frequency of the first mode while increasing the frequency of the second mode as will also be deduced from the shape perturbation equation [24].

$$\frac{\omega_u - \omega_p}{\omega_u} \approx \frac{\int_{\Delta V}(\varepsilon|\vec{E}|^2 - \mu|\vec{H}|^2)dv}{\int_{V_0}(\varepsilon|\vec{E}|^2 + \mu|\vec{H}|^2)dv} \tag{62}$$

where $\vec{E}$, $\vec{H}$, ε and μ denote the electric and magnetic field vectors of the corresponding mode, dielectric permittivity and magnetic permeability, respectively. V_0 is the cavity volume, and ΔV indicates the perturbation volume. In this case, when an inward perturbation is applied from the region where the electric field peaks, the value of $\omega_u - \omega_p$ remains positive. This implies a decrease in frequency. Similarly, due to the minus sign in front of the magnetic field in the denominator, when the same operation is applied to the region where the magnetic field peaks, the frequency increases.

When we handle a rectangular cavity whose dimensions are $b = 11$ cm, $a = d = 26.5$ cm, its dominant mode is located at 800 MHz and the frequency

of the second mode exceeds a slightly higher value than 1.26 GHz, which lies at the limit we have analytically found. In the previous section, the condition $a = d \geq 2b$ was found to hold, which enables us to obtain a frequency ratio at the limit values. It is important to note that the measurement should be carried out using weak coupling ensuring that the coupling loops do not significantly distort the shape of the rectangular prism. In effect, while the initial ratio between the frequencies of the first two modes of the rectangular cavity is 1.58, the employment of an internal perturbation from the center of the structure may serve to elevate this proportion; see Fig. 3-(a). The selected perturbing object for this structure is cylindrical in shape with a diameter of 3.5 cm and an inserted height of 4.5 cm. The limitations determined pertain solely to the case of a perfect rectangular prism and a perfect cylinder. The surmounting of these limits can be envisioned if and when the idealized conditions of such geometries are compromised.

A similar analysis has been conducted for cylindrical cavities; see Fig. 3-(b). A cylindrical cavity with a radius of 7 cm and a height of 4.4 cm was measured with weakly coupled two identical couplers. As a result of selecting these dimensions, the conditions $\frac{-2.395}{r^2} + \frac{\pi^2}{l^2} \geq 0$ and $\frac{11.295}{r^2} - \frac{\pi^2}{l^2} \leq 0$ were satisfied. The initial two modes were separated from each other by inserting a conical perturbing object into the top of the cylindrical cavity. The height of the inserted cone was 2.6 cm, with a top radius of 0.2 cm and a bottom radius of 1.1 cm.

A check was performed in Fig. 4 to ascertain if there were any limitations regarding the sizes of objects that would penetrate inward from the cavity centers. To assess the feasibility of different shapes, a cylindrical object was placed in the rectangular cavity, and a conical object was placed in the cylindrical cavity, with their sizes varied to observe the resonance frequencies of the first two modes. For the perturbing cylinder in the rectangular cavity, simulations were conducted with three different length values, namely 10, 30, and 50 mm, and for various diameter values in increments of 10 mm, ranging from 10 to 80 mm. Regarding the conical object in the cylindrical cavity, the top radius was kept constant, while the bottom diameter and length were varied within the ranges of 10-30 and 10-60, respectively. As the size of the perturbing object increases, the first mode's frequency decreases in both cavity types, aligning with the intended objective. For the second mode, an increase in frequency is observed, and there's a potential for the mode frequencies to separate when the perturbing object has a relatively small diameter. Once the perturbing object's diameter surpasses a specific threshold, it initiates disruptions in the electric field of the dipole mode, leading to a reduction in frequency.

4.2 The Proposed Cavity and the Results

In Computer Simulation Technology - Microwave Studio (CST-MWS) software, utilizing a macro for elliptical cavity design, the dimensions shown in Fig. 5-(a) were drawn and meticulously optimized through detailed analyses. These dimensions were specified in millimeters. Along with these dimensions, the ratio of the second mode's frequency to the first mode's frequency was calculated to be

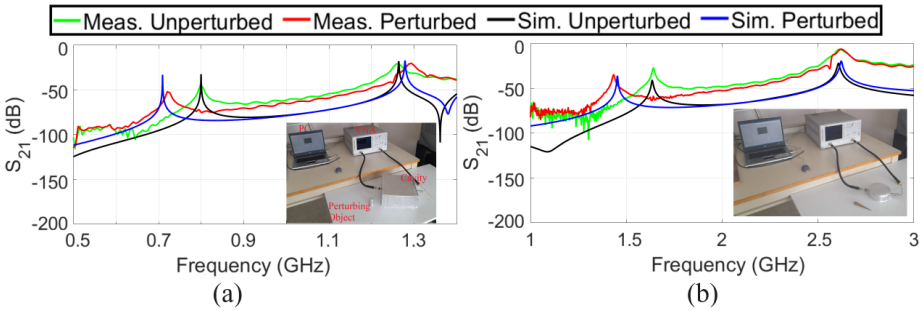

Figure 3: Numerical and experimental results of the unperturbed and perturbed (a) rectangular cavity (b) cylindrical cavity

approximately 2.37, achieving the desired mode frequency ratio. Subsequently, the drawn structure was uniformly scaled in all three dimensions with a scaling factor of 0.166. As a result, a structure was obtained with the first mode at 2.45 GHz and the second mode at 5.8 GHz, with no possibility of exciting any mode physically between these frequencies. This structure represents a half-cell and requires the addition of another one with mirror symmetry. Along with the holes for eight screws, two tuner and two N-type couplers, the final configuration can be seen in Fig. 5-(b)-(f).

The electric field patterns for the first two modes can be observed in Fig. 6. In the context of the aforementioned applications, the deliberate separation of the frequencies of the first two modes serves to prevent spectral overlap caused by frequency shifts during permittivity or permeability measurements or any other cavity-based measurement system, thus avoiding interference between closely positioned modes in the frequency domain.

The degree of enhancement with the proposed cavity is better understood through a comparison with rectangular and cylindrical cavities. To achieve this, simulations of rectangular and cylindrical cavities that adhere to the maximum mode frequency ratio from the preceding sections, and that host the first mode at 2.45 GHz, were conducted. To address this, frequency domain calculations were conducted using CST-MWS software for each cavity type, employing two N-type couplers and two loop antennas. Smith chart graphs were generated to visualize impedance values for the first ports. As evident in Fig. 7-(a) and -(b), when rectangular and cylindrical cavities are employed, a significant number of modes are excited within the 2-6.5 GHz range, and these modes exhibit intricate overlap in the respective graphs. As depicted in Fig. 7-(c), the Smith chart representation of the proposed cavity within the 2-6.5 GHz range with two slightly under coupled modes is provided. In comparison to the other two cavities, it exhibits a notably distinct and unambiguous pattern, which restricts intermodal crosstalk.

The cavity was produced in two parts using a 3D printer and PLA material via the fused deposition modeling (FDM) technology. The interior of the cavity

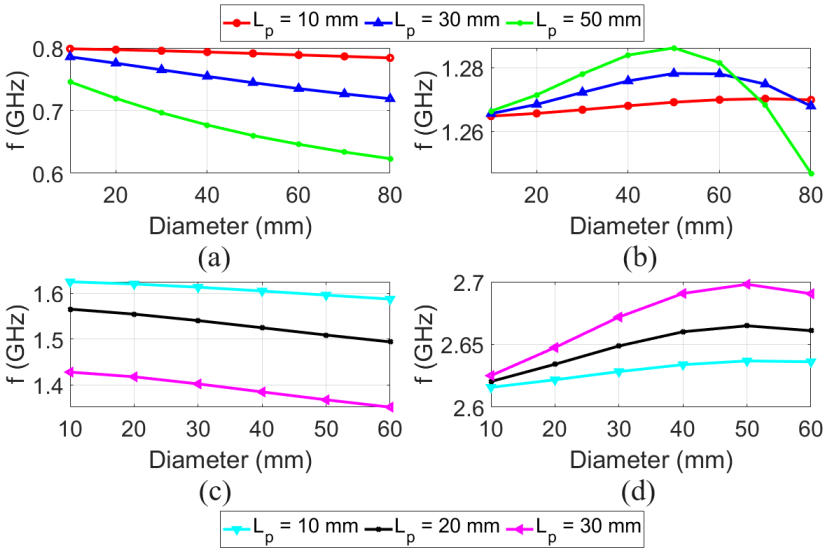

Figure 4: Parametric study for frequency shift of rectangular and cylindrical cavities with various size of perturbing objects (L_p: length of the perturbing object) (a) mode-1 of rectangular cavity with a cylindrical object (b) mode-2 of rectangular cavity with a cylindrical object (c) mode-1 of cylindrical cavity with a conical object (top radius of the cone is fixed to 2 mm) (d) mode-2 of cylindrical cavity with a conical object (top radius of the cone is fixed to 2 mm)

was made conductive through the application of a conductive aerosol coating method, followed by sealing the cavity using the screw holes; see Fig. 8. The N-type coupler holes of the cavity allow the convenient placement of couplers with small loop antennas soldered at their ends, enabling the portable arrangement for cavity excitation. On both parts of the cavity, plastic tubes, shaped like cones, are inserted into tuner holes with a 4 mm diameter and filled with liquid metal to a desired level. This procedure aims to compensate for frequency shifts arising from production errors or coating-related factors. Furthermore, this procedure, employing about two grams of gallium and a syringe, has been introduced as an innovative approach to cavity tuner design. Leveraging the liquid metal-assisted tuning method, which offers greater flexibility compared to conventional mechanical tuners, the frequencies of the first two modes have been adjusted to 2.45 and 5.8 GHz, as evidenced by measurement results.

The dimensions of the conventional cavities, with their first mode frequencies set at 2.45 GHz, were determined to achieve the maximum frequency separation according to the aforementioned analytical calculations. The S_{21} results of the structures excited by dual ports in the simulation environment are illustrated in Fig. 9-(a). Utilizing such structures with a plethora of closely spaced modes ranging from 2 to 6.5 GHz is not sufficiently functional for measurements requiring separated mode frequencies. Conversely, Fig. 9-(b) presents the weakly

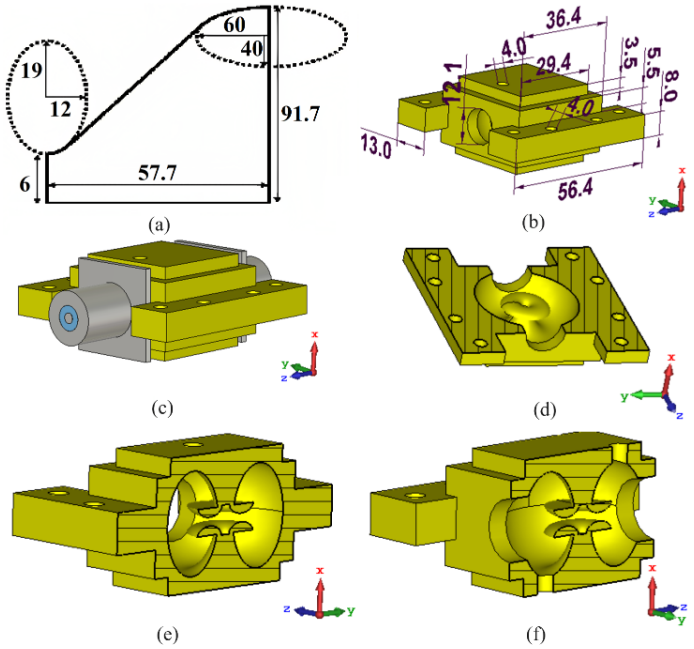

Figure 5: Design of the proposed cavity (a) elliptical cavity curve of half-cell in mm before scaling of 0.166 (b) final outer dimensions in mm (c) with the N-type couplers (d) cross-sections on yoz plane (e) xoy plane (f) xoz plane

coupled (coupling coefficient ≈ 0.09 & 0.04, respectively) S_{21} simulation results of the proposed cavity, along with the measurement outcome of the cavity whose frequency has been precisely adjusted to the desired values using the liquid metal tuner. Furthermore, single-port critical coupling (coupling coefficient ≈ 1 for both modes) measurements were taken, as shown in Fig 9-(c). While critical coupling measurements may introduce minor frequency variations, the higher measured power level results in a more closely matched graphical representation. According to these results, the proposed structure offers a significantly distinct and non-overlapping graph in comparison to conventional designs. Although there is some broadening in the peaks and dips in the measurements due to lower conductivity values compared to the simulation, the modes appear sufficiently separated in the spectral domain.

The comparison of the proposed cavity with rectangular and cylindrical cavities is presented in Table 1. When the dominant modes of all three cavities are set to 2.45 GHz, the second mode of the rectangular and cylindrical cavities can reach a limited value. However, in the proposed cavity, the second mode is located at 5.8 GHz. By filling the holders placed in 4 mm diameter tuner holes with liquid metal tuner, the frequency of the first mode can be adjusted between 2.43 and 2.47 GHz, while the frequency of the second mode can be varied between 5.77 and 5.82 GHz. In other words, by using tuners, the mode

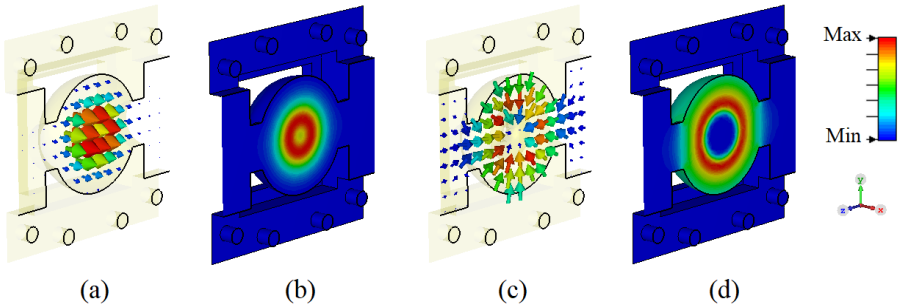

Figure 6: Electric field patterns of the proposed cavity (a) vector arrows of the first mode at 2.45 GHz (b) contour plot of the first mode at 2.45 GHz (c) vector arrows of the second mode at 5.8 GHz (d) contour plot of the second mode at 5.8 GHz

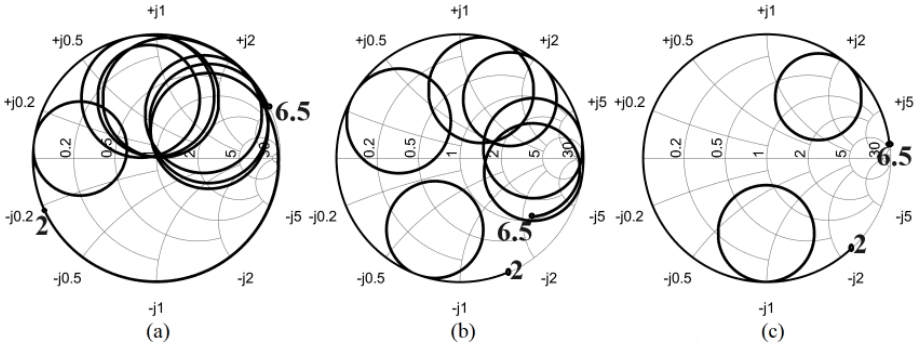

Figure 7: Smith chart between 2 GHz and 6.5 GHz (a) rectangular cavity (b) cylindrical cavity (c) proposed cavity

frequencies placed at 2.45 GHz and 5.8 GHz can be separated by up to 40 MHz, if desired. Upon conducting a comparative analysis of the cross-sectional areas within the interior of the cavities, it becomes apparent that the proposed cavity has a rather small electrical size. According to simulations conducted in CST-MWS, the quality factors of the proposed cavity, assuming the walls are made of copper, are found to be 3150 and 3750 for the first two modes, respectively. The quality factors of the cylindrical and rectangular cavities are highly dependent on their volumes. To facilitate a fair comparison, configurations were considered in which the internal volumes were kept equal without violating the condition in the equations above. Taking into account that the internal volume of the proposed cavity is approximately 10800 mm^3, the cross-sectional dimensions of the rectangular cavity are chosen as $d = a = 86.6$ mm to bring the first mode to 2.45 GHz, with b to be less than 43.3. As for the cylindrical cavity, a radius of 46.8 mm is required, and the height value should be selected in a way that doesn't violate the condition mentioned above. If dimensions are

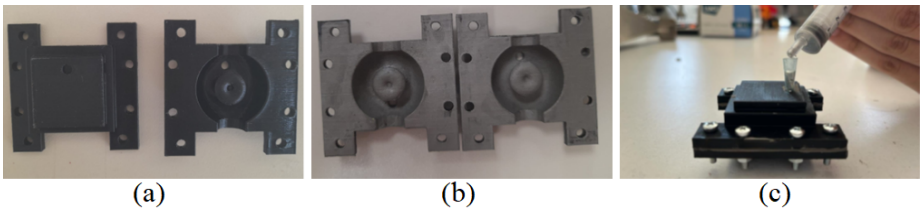

Figure 8: Additively manufactured cavity (a) uncoated half-cells (b) half-cells after aerosol coating (c) tuning with liquid metal

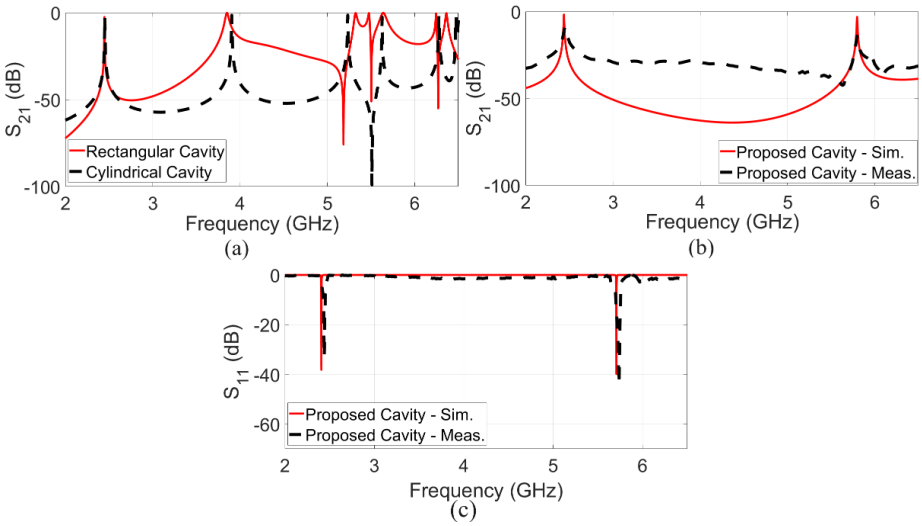

Figure 9: Scattering parameters of (a) S_{21} of simulated rectangular and cylindrical cavities whose dominant modes are at 2.45 GHz (b) S_{21} of simulated and measured proposed cavity with weak coupling (c) S_{11} of simulated and measured proposed cavity with critical coupling

chosen to maintain the same internal volume that is approximately 10800 mm^3, the quality factor values for the first two modes of the rectangular cavity are determined to be 1050 and 1310, respectively, while for the cylindrical cavity, these values are found to be 1160 and 1460.

5 Conclusion

This study addresses the critical challenge of enhancing measurement accuracy and mitigating the impact of neighboring modes in resonant cavities. The initial analytical investigation, utilizing Lagrange multipliers, provides a perspective on the achievable extent of mode separation within conventional cavities. The limits about 1.581 for rectangular and 1.593 for cylindrical are insufficient for

Table 1: Comparison between the conventional cavities and the proposed cavity

Cavity Shape	Rectangular	Cylindrical	Proposed
1^{st} mode frequency	2.45 GHz	2.45 GHz	2.45 GHz
2^{nd} mode frequency	3.86 GHz	3.90 GHz	5.8 GHz
Ratio	1.58	1.59	2.37
Cross-sectional area	74.82 cm^2	68.81 cm^2	7.25 cm^2
Q (same inner volume)	1050-1310	1160-1460	3150-3750

the placement of the first two modes at 2.45 and 5.8 GHz within the ISM band measurement systems. The resultant ratios were also validated via grid search and align with literature charts. Furthermore, we experimentally surpassed these limits by perturbing cavity geometry, creating a novel structure with a small electrical size, tunable via liquid metal. This innovation positioned the first mode at 2.45 GHz and the second mode at 5.8 GHz, eliminating undesired intermediary modes beyond the ISM band. Moreover, the article showcases the tunability of the proposed cavity structure through the use of liquid metal displacement, unlocking a more flexible tuning method compared to traditional mechanical approaches. These achievements significantly enhance measurement accuracy for diverse applications (e.g. single band dielectric permittivity or permeability measurements) requiring isolated modes.

References

[1] Q. Shi, Q.-X. Chu, M.-Z. Xiao, F.-C. Chen, X.-Q. Huang, and X. He, "Complex permittivity measurement utilizing multiple modes of a rectangular cavity," *IEEE Transactions on Instrumentation and Measurement*, vol. 72, pp. 1–8, 2022.

[2] J. D. Gutiérrez-Cano, P. Plaza-González, A. J. Canós, B. García-Baños, J. M. Catalá-Civera, and F. L. Peñaranda-Foix, "A new stand-alone microwave instrument for measuring the complex permittivity of materials at microwave frequencies," *IEEE Transactions on Instrumentation and Measurement*, vol. 69, no. 6, pp. 3595–3605, 2019.

[3] A. K. Jha and M. J. Akhtar, "A generalized rectangular cavity approach for determination of complex permittivity of materials," *IEEE Transactions on Instrumentation and Measurement*, vol. 63, no. 11, pp. 2632–2641, 2014.

[4] J. Krupka, "Frequency domain complex permittivity measurements at microwave frequencies," *Measurement Science and Technology*, vol. 17, no. 6, p. R55, 2006.

[5] C. Özkal and F. Yaman, "A non-resonant approach for dielectric constant reconstructions via newton iterations," *AEU-International Journal of Electronics and Communications*, p. 154802, 2023.

[6] A. K. Jha and M. J. Akhtar, "An improved rectangular cavity approach for measurement of complex permeability of materials," *IEEE Transactions on Instrumentation and Measurement*, vol. 64, no. 4, pp. 995–1003, 2014.

[7] D. Gouveia, L. Costa, and M. Valente, "Resonant cavity for the measurement of microwave magnetic permeability using the small perturbation theory," *Microwave and Optical Technology Letters*, vol. 50, no. 2, pp. 399–402, 2008.

[8] Z. Li, C. Wu, Z. Meng, C. Soutis, Z. Chen, P. Wang, and A. Gibson, "Accurate thickness measurement of multiple coating layers on carbon fiber composites using microwave cavity perturbation," *IEEE Transactions on Instrumentation and Measurement*, vol. 71, pp. 1–10, 2022.

[9] W. Xiao, Y. Liao, and K. Huang, "Measuring electron density of atmospheric microwave plasma jet by microwave perturbation method," *IEEE Transactions on Instrumentation and Measurement*, vol. 71, pp. 1–9, 2022.

[10] S. N. Kharkovsky and U. C. Hasar, "Measurement of mode patterns in a high-power microwave cavity," *IEEE Transactions on Instrumentation and Measurement*, vol. 52, no. 6, pp. 1815–1819, 2003.

[11] M. Forouzanfar and M. Joodaki, "Systematic design of hybrid high power microwave amplifiers using large gate periphery gan hemts," *AEU-International Journal of Electronics and Communications*, vol. 84, pp. 225–233, 2018.

[12] Y. Jiang, H. Zha, J. Shi, M. Peng, X. Lin, and H. Chen, "A compact X-Band microwave pulse compressor using a corrugated cylindrical cavity," *IEEE Transactions on Microwave Theory and Techniques*, vol. 69, no. 3, pp. 1586–1593, 2021.

[13] V. Goryashko, M. Jobs, L. Duc, J. Ericsson, and R. Ruber, "12-way 100 kw reentrant cavity-based power combiner with doorknob couplers," *IEEE Microwave and Wireless Components Letters*, vol. 28, no. 2, pp. 111–113, 2018.

[14] T. Steinmetz, T. Wilken, C. Araujo-Hauck, R. Holzwarth, T. W. Hansch, and T. Udem, "Fabry-perot filter cavities for wide-spaced frequency combs with large spectral bandwidth," *Applied Physics B*, vol. 96, pp. 251–256, 2009.

[15] J. Robinson, S. Kingman, D. Irvine, P. Licence, A. Smith, G. Dimitrakis, D. Obermayer, and C. O. Kappe, "Understanding microwave heating effects in single mode type cavities—theory and experiment," *Physical Chemistry Chemical Physics*, vol. 12, no. 18, pp. 4750–4758, 2010.

[16] S. Curet, O. Rouaud, and L. Boillereaux, "Microwave tempering and heating in a single-mode cavity: Numerical and experimental investigations," *Chemical Engineering and Processing: Process Intensification*, vol. 47, no. 9-10, pp. 1656–1665, 2008.

[17] O. Dutta, M. Jääskeläinen, and P. Meystre, "Single-mode acceleration of matter waves in circular waveguides," *Physical Review A*, vol. 74, no. 2, p. 023609, 2006.

[18] C. A. Balanis, *Advanced engineering electromagnetics*. John Wiley & Sons, 2012.

[19] A. Karatay and F. Yaman, "Electromagnetic simulations of mechanical imperfections for accelerator cavities," *IEEE Transactions on Nuclear Science*, vol. 66, no. 11, pp. 2295–2304, 2019.

[20] A. Karatay, H. Ö. Yılmaz, C. Özkal, and F. Yaman, "Cost-effective experiments with additively manufactured waveguide and cavities in the s-band," *Measurement Science and Technology*, vol. 34, no. 8, p. 085904, 2023.

[21] K. N. Paracha, A. D. Butt, A. S. Alghamdi, S. A. Babale, and P. J. Soh, "Liquid metal antennas: Materials, fabrication and applications," *Sensors*, vol. 20, no. 1, p. 177, 2019.

[22] W. L. Winston, M. Venkataramanan, and J. B. Goldberg, *Introduction to mathematical programming*. Thomson/Brooks/Cole Duxbury, Pacific Grove, CA, 2003, vol. 1.

[23] D. A. Hill, *Electromagnetic fields in cavities: deterministic and statistical theories*. John Wiley & Sons, 2009.

[24] D. M. Pozar, *Microwave Engineering*. John Wiley & Sons, 2011.